

Straightforward electrical measurement of forward-voltage to investigate thermal effects in InGaN/GaN high-brightness light-emitting diodes

Bobby Logan Hancock, and Mark Holtz

Citation: *Journal of Vacuum Science & Technology B* **32**, 061209 (2014); doi: 10.1116/1.4901411

View online: <https://doi.org/10.1116/1.4901411>

View Table of Contents: <https://avs.scitation.org/toc/jvb/32/6>

Published by the [American Vacuum Society](#)

ARTICLES YOU MAY BE INTERESTED IN

[Junction-temperature measurement in GaN ultraviolet light-emitting diodes using diode forward voltage method](#)
Applied Physics Letters **85**, 2163 (2004); <https://doi.org/10.1063/1.1795351>

[Bulk GaN flip-chip violet light-emitting diodes with optimized efficiency for high-power operation](#)
Applied Physics Letters **106**, 031101 (2015); <https://doi.org/10.1063/1.4905873>

[III-nitrides: Growth, characterization, and properties](#)
Journal of Applied Physics **87**, 965 (2000); <https://doi.org/10.1063/1.371971>

[Effect of electron blocking layer on efficiency droop in InGaN/GaN multiple quantum well light-emitting diodes](#)
Applied Physics Letters **94**, 231123 (2009); <https://doi.org/10.1063/1.3153508>

[Defect related issues in the "current roll-off" in InGaN based light emitting diodes](#)
Applied Physics Letters **91**, 181103 (2007); <https://doi.org/10.1063/1.2801704>


[Improved brightness of 380 nm GaN light emitting diodes through intentional delay of the nucleation island coalescence](#)
Applied Physics Letters **81**, 1940 (2002); <https://doi.org/10.1063/1.1506793>



Instruments for Advanced Science

Contact Hiden Analytical for further details:
W www.HidenAnalytical.com
E info@hiden.co.uk

CLICK TO VIEW our product catalogue




Gas Analysis

- dynamic measurement of reaction gas streams
- catalysis and thermal analysis
- molecular beam studies
- dissolved species probes
- fermentation, environmental and ecological studies




Surface Science

- UHV TPD
- SIMS
- end point detection in ion beam etch
- elemental imaging - surface mapping



Plasma Diagnostics

- plasma source characterization
- etch and deposition process reaction kinetic studies
- analysis of neutral and radical species



Vacuum Analysis

- partial pressure measurement and control of process gases
- reactive sputter process control
- vacuum diagnostics
- vacuum coating process monitoring

Straightforward electrical measurement of forward-voltage to investigate thermal effects in InGaN/GaN high-brightness light-emitting diodes

Bobby Logan Hancock^{a)}

Materials Science, Engineering, and Commercialization, Texas State University, 601 University Dr., San Marcos, Texas 78666

Mark Holtz

Department of Physics and Materials Science, Engineering, and Commercialization, Texas State University, 601 University Dr., San Marcos, Texas 78666

(Received 8 October 2014; accepted 29 October 2014; published 12 November 2014)

The junction temperature of InGaN/GaN MQW high-brightness light-emitting diodes is measured using an electrical method based on the dependence of diode forward voltage, V_f , on the junction temperature T_j . Electroluminescence (EL) data collected during this measurement are presented and used to compare the efficacy of this method for measuring T_j to the electrical technique. In devices based on polar III-nitride materials, the temperature dependence of the EL peak energy is obscured by carrier screening and bandfilling; the contributions of these effects are explored and presented. Additionally, the experimental method presented offers an application for extrapolating a thermal relaxation time during the junction temperature measurement. The results from this thermal time constant study are presented and discussed. © 2014 American Vacuum Society.

[<http://dx.doi.org/10.1116/1.4901411>]

I. INTRODUCTION

III-nitride materials have proven to be valuable in light-emitting diodes (LEDs) in the violet to near-ultraviolet (UV) wavelength range. Self-heating in the active region of these devices is a critical concern as it directly affects the internal quantum efficiency, peak emission energy, degradation, and overall operating lifetime. For this reason, monitoring the junction temperature in these devices is important.

Spectroscopic measurements of the junction temperature can be accomplished several ways, including Raman,¹ photoluminescence,² and electroluminescence (EL).³ Apart from the experimental complexity of these measurement schemes, spectroscopic measurements reliant on the temperature-induced changes in band gap energy suffer from competition with carrier screening and bandfilling in polar III-nitride materials.

Xi and Schubert⁴ presented an indirect method for establishing junction temperature based on the temperature dependence of the diode forward voltage in the active region for UV GaN LEDs. This method was extended and modified by Keppens *et al.*,⁵ who demonstrated an alternative experimental technique based on similar semiconductor principles for various packaged III-V LEDs.

The study presented here involves an experimental determination of junction temperature for packaged InGaN/GaN MQW high-brightness LEDs. The experimental approach is simplified when compared with previous reports⁴⁻⁶ and the expression derived for the forward voltage temperature dependence avoids use of an empirical band gap dependence. An investigation of the effects of bandfilling and carrier screening on the electroluminescence in these devices is also explored, offering a verification of the efficacy of the

forward voltage method as compared to spectroscopic techniques. Finally, the experimental setup utilized in this study provides an alternative means for extrapolating the thermal time constant for the material during the junction temperature measurement.

II. EXPERIMENTAL DETAILS

Commercially available high-brightness, blue (475 nm) InGaN/GaN MQW LEDs were investigated. Forward voltage and drive current measurements were accomplished using a Keithley 2400 SourceMeter in conjunction with a NI PCI-4472 data acquisition (DAQ) board voltmeter controlled via custom LABVIEW programs. Temperature calibration was performed with the LED mounted on a heat sink inside a standard temperature-controlled laboratory furnace. For electroluminescence measurements, the LED output emerging from a small aperture in the furnace wall was collected and focused into the fiber optic cable of a miniature spectrometer. Wavelength calibration is verified using standard sources.

III. FORWARD VOLTAGE METHOD

Figure 1(a) shows forward voltage, V_f , versus oven temperature obtained for calibrating the effect of junction temperature (T_j) on V_f . For these measurements, the LED was mounted on a heat sink inside a conventional laboratory oven. Temperature was set and, after reaching the set point, allowed to stabilize prior to each voltage measurement. A drive current of 2.0 mA at a frequency of 0.33 Hz with a 0.1% duty cycle was used to minimize current-induced self-heating. A schematic of this pulsed drive current is shown in the inset of Fig. 1(a). The dependence in Fig. 1(a) allows us to obtain the negative linear temperature coefficient $\kappa = dV_f/dT$ as in Refs. 3 and 4

^{a)}Electronic mail: bobby.hancock@txstate.edu

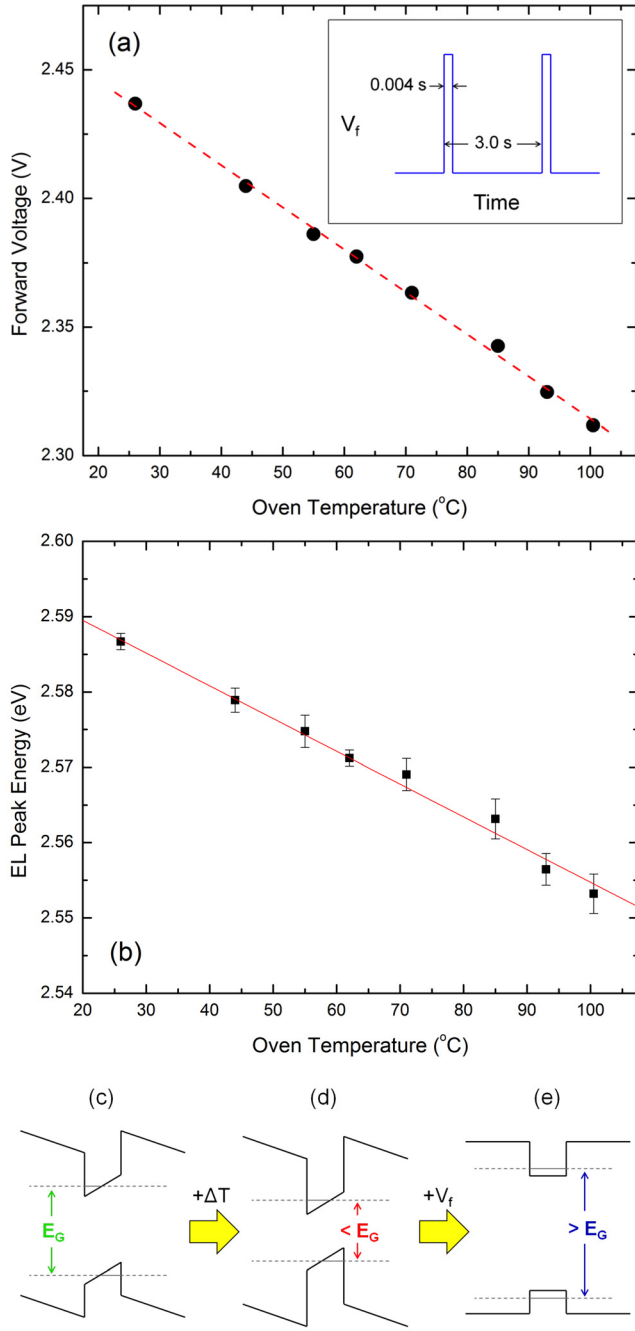


FIG. 1. (Color online) Results from calibration step of forward voltage method. (a) Calibration of measured forward voltages for controlled changes in ambient temperature. The inset illustrates the pulsed current used to operate the device while minimizing self-heating. (b) Electroluminescence peak energies obtained during the calibration voltage measurement. (c) Depiction of band edges in polar InGaN MQW without external drive. (d) and (e) qualitatively illustrate the effects of just temperature increase and voltage-induced carrier screening on changes in the band gap energies, respectively.

$$V_f = V_0 + \kappa T_j. \quad (1)$$

Once the linear regression in Eq. (1) has been established experimentally, the junction temperature T_j is readily obtained based on subsequent measurements. We obtained a value of $\kappa = -1.64 \pm 0.03$ mV/K for the device studied, in good agreement with previously published results on GaN-based LEDs.^{3–5,7,8}

Figure 1(b) summarizes the temperature dependence of the EL emission peak. These measurements were carried out simultaneously with the calibration measurement discussed above, under identical low current drive conditions to avoid unwanted self-heating. Because the current is kept low during calibration, the emission is low in intensity. However, reasonable spectra are obtained over multiple cycles using an open shutter approach and a systematic red shift is obtained with slope $dE_g/dT = -0.43 \pm 0.01$ meV/K. Because these data were obtained under low drive conditions, this shift corresponds to the temperature dependence alone. In nonpolar quantum well structures, the EL shift may be used to determine device temperature even under normal operating conditions, as previously demonstrated in GaAs-based LEDs.^{5,9,10} As discussed in Sec. VI, this is not the case for InGaN quantum wells due to screening of the built-in field and bandfilling at high drive current. Figures 1(c)–1(e) qualitatively depict the separate effects of heating-induced shrinkage of the band gap and carrier screening under applied forward bias. These effects combine to shift the overall EL peak, thereby preventing the straightforward use of optical measurements to estimate temperature rise in polar devices.

IV. CALCULATIONS

The forward voltage temperature coefficient has been previously investigated.^{4,5} Based on the Shockley diode equation, Xi and Schubert⁴ show that

$$e \frac{dV_f}{dT} \approx k_B \ln \frac{N_D N_A}{N_C N_V} + \frac{dE_g}{dT} - 3k_B, \quad (2)$$

where N_D and N_A represent the donor and acceptor concentrations for electrons, respectively. N_C and N_V are effective densities of states at the conduction and valence band edges, respectively. E_g is the temperature-dependent energy gap, k_B is the Boltzmann constant, and e is the elementary charge. Here, we describe the temperature dependence of E_g based on the phonon occupation^{11,12} rather than the empirical Varshni model. When the electron–phonon interactions may be grouped into acoustic and optic branches, the band gap shifts according to

$$E_g(T) = E_g(0) - \frac{\delta}{k_B} \{ W_{ac} \varepsilon_{ac} n(\varepsilon_{ac}, T) + W_{opt} \varepsilon_{opt} n(\varepsilon_{opt}, T) \} - \int_0^T [\xi_c \alpha_c(T') + 2\xi_a \alpha_a(T')] dT', \quad (3)$$

where δ is the high-temperature slope of the band gap, W_{ac} (W_{opt}) the acoustic (optic) phonon weighting factor subject to $W_{ac} + W_{opt} = 1$, ε_{ac} (ε_{opt}) the acoustic (optic) phonon energy, and n is the Bose function. The last term in Eq. (3) accounts for thermal expansion; deformation potentials along the c (a) crystal axis of the active region material are ξ_c (ξ_a) and the corresponding thermal expansion coefficients are α_c (α_a). Across the temperature range studied here, this integral term in Eq. (3) is negligible in comparison to the quantity in brackets.¹³ In the temperature range where $k_B T > \varepsilon_{ac}$ the first term in brackets may be approximated as

$W_{ac}k_B T$. In GaN, for which the phonon spectrum is similar to that of InGaN, $\epsilon_{ac} \sim 22.5$ meV corresponding to a temperature of 260 K.¹³ At even higher temperature, $k_B T > \epsilon_{opt}$ and the second term in brackets becomes $W_{opt}k_B T$. The value of $\epsilon_{opt} \sim 69.3$ meV in GaN with a corresponding temperature of 800 K.¹³ For temperatures in this high range, the term in brackets in Eq. (3) simplifies to $k_B T$ so that we retrieve the linear dependence $E_g(T) \approx E_g(0) - \delta T$.

Values in the range 0.1 – 0.5 meV/°C have been reported in the literature for δ in InGaN.^{5,7,10,14–16} Despite our measurements being in the intermediate temperature range $\epsilon_{ac} < k_B T < \epsilon_{opt}$, our value of $\delta \approx 0.43$ meV/°C is reasonably within the published range.

A value for dV_f/dT can be calculated from Eq. (2) using our value for $\delta \approx 0.43$ meV/°C, assuming $N_D = N_A = 2 \times 10^{16}$ cm⁻³ and using GaN values for $N_C \approx (4.3 \times 10^{14}) T^{3/2}$ cm⁻³ and $N_V \approx (8.9 \times 10^{15}) T^{3/2}$ cm⁻³ from Ref. 4

$$e \frac{dV_f}{dT} \approx k_B \ln \frac{N_D N_A}{N_C N_V} - \delta - 3k_B. \quad (4)$$

This results in a slope $dV_f/dT \approx -1.77$ mV/°C for this type of device, in agreement with the measured value of -1.64 ± 0.03 mV/K from Fig. 1(a).

V. JUNCTION TEMPERATURE RESULTS

The junction temperature was measured with the LED mounted in thermal contact with a standard heat sink and driven at a specified current ranging from 10 to 600 mA. DC current at this value was initially applied for 2 min to establish steady-state conditions, as monitored via the V_f value. The current was then abruptly switched to 2 mA to match what was used in the calibration step, as illustrated in the inset of Fig. 2. By taking a forward voltage measurement at the low current, the linear regression obtained from

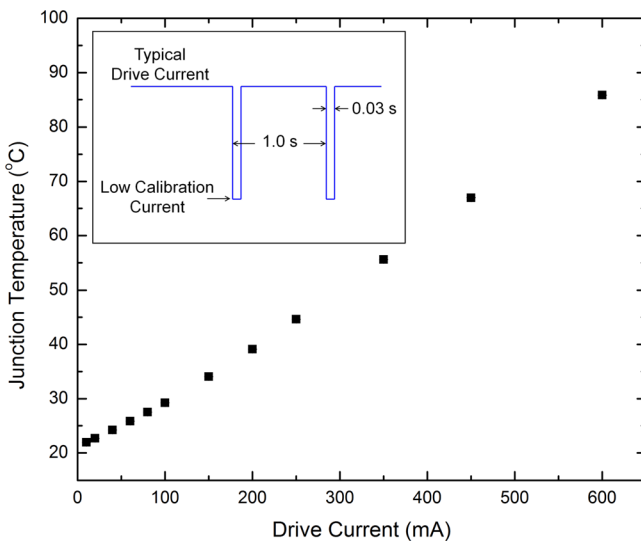


Fig. 2. (Color online) Measured junction temperature values for various LED drive currents. The inset illustrates the lineshape of the applied drive current; the junction temperature is measured in the notch when low calibration current is applied.

calibration, Fig. 1(a), can be used to calculate the junction temperature for the LED. The DAQ voltmeter has a sampling rate of 20 000 samples/s giving a time resolution of 50 μ s for the instrument. Delays in the current source upon changing from high to low drive conditions become the limiting factor in the junction temperature determination. Considering this, we find that V_f can be accurately established within 3 ms after switching to low current, allowing the setup time to pass the Gibbs overshoot while preceding significant cooling in the active region. In Fig. 2, we show results of the dynamic junction temperature measurement as a function of drive current. The T_j increase is slightly faster than linear with current due to the diminishing thermal conductivity as temperature increases and the higher fraction of input power generating heat rather than optical output.

VI. EFFECTS OF SELF-HEATING ON EL SPECTRUM

Figure 3(a) shows EL spectra obtained at different drive currents under identical conditions to those used for

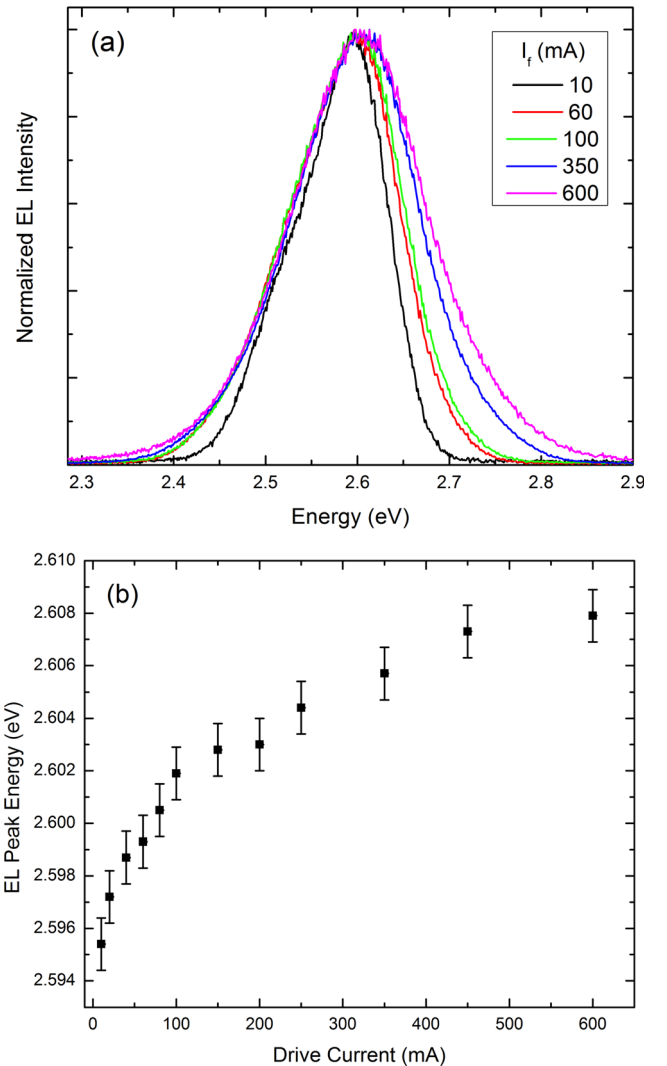


Fig. 3. (Color online) Electroluminescence data for typical drive currents. (a) EL spectra collected during the junction temperature measurement. (b) Summary of the EL peak energies at each applied drive current during the measurement.

measuring T_j . The low-current spectrum shows an EL peak at 2.595 eV. As drive current is increased, intensity rises and we observe a systematic blue shift in the EL peak position. The blue shift is seen clearly in Fig. 3(b), where we plot EL peak energy as a function of drive current. Since T_j is increasing with drive current (Fig. 2), and the band gap in Fig. 1(b) shows a red shift with increasing temperature, the observed blue shift is not attributable to a rise in temperature. Bandfilling is one possible cause for the overall shift, an effect which would also result in broadening of the EL emission.^{7,17–19} In addition, the blue shift is expected from carrier-induced screening of the built-in field within the (0001)-oriented III-nitride quantum wells.^{17,19}

VII. EFFECTS OF SCREENING AND BANDFILLING ON EL

As previously illustrated in Figs. 1(c)–1(e), the combined effects of bandfilling and carrier screening make a significant contribution to the behavior of the EL spectrum for InGaN MQW devices; this can be seen in the data in Fig. 3(b). The influence of these effects is further demonstrated in Fig. 4. The square data points represent the shift in EL peak energies from Fig. 3(b) relative to the room-temperature peak position. The solid curve corresponds to the expected shift in EL peak energy due to temperature rise; the T_j values are measured at each drive current. This was determined using the linear trend from Fig. 1(b) for temperature-induced band gap shrinkage. The diamond data points are the result of correcting the measured shift (in black) for the effects of temperature on the band gap to illustrate the effects of bandfilling and screening. As deduced from the plot, bandfilling plus carrier screening impart a relative blue shift of approximately 28 meV on the EL for these devices. This illustrates the necessity for using an electrical approach, like

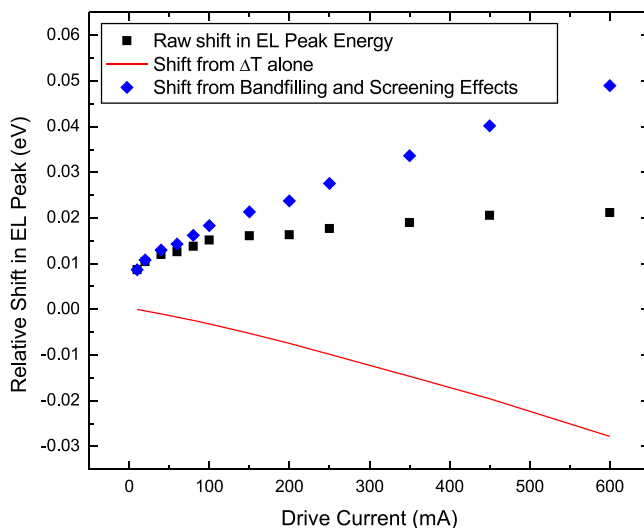


Fig. 4. (Color online) Demonstration of the effects of bandfilling and carrier screening on the EL output. Square data points (black online) represent the relative shift of the EL peak energies. The solid curve (red online) shows the expected shift for only temperature-induced changes in the band gap energy based on data in Fig. 1. Diamond data points (blue online) show the effect of bandfilling and carrier screening.

the forward voltage method, for determining the junction temperature in InGaN LEDs (and similar devices based on other polar semiconductors) as opposed to measurements based solely on EL measurements.

VIII. EXTRACTION OF THERMAL TIME CONSTANT

Heat generated in the LED active region due to nonradiative recombination and resistive losses is transferred to the substrate by means of thermal conduction. The time-dependence of this heat transfer can be described by the familiar relation

$$\frac{dQ}{dt} = hA(T(t) - T_{\text{ambient}}), \quad (5)$$

where dQ/dt represents a heat flux, h is the heat transfer coefficient in units $\text{W}/\text{m}^2\text{K}$, and A represents the surface area where the heat flux takes place. Expressing this in terms of the heat capacity, C , of the material under the assumption that $C = dQ/dT$ and using the thermodynamic relationship $dQ/dt = C(dT/dt)$, the above relation can be rewritten

$$\frac{dT(t)}{dt} = -\frac{hA}{C}(T(t) - T_{\text{ambient}}) \equiv -\frac{1}{\tau} \Delta T(t). \quad (6)$$

The quantity C/hA corresponds to a thermal time constant, τ , characteristic of the device and the term $\Delta T(t) = T(t) - T_{\text{ambient}}$. The solution to this differential equation can be written as

$$\Delta T(t) \sim \exp\left(-\frac{t}{\tau}\right). \quad (7)$$

When multiple factors contribute to the cooling, each with different time constants τ_i , they may be taken into account by adding further terms to Eq. (7) with coefficients β_i corresponding to their relative contributions. For the case of III–V LEDs, identification of the thermal time constant is useful as this material-characteristic value gives insight into the underlying behavior of the heat dissipation throughout the device. In Ref. 20, Vitta and Žukauskas present a method for extracting the time constant in various LED materials using a frequency modulation technique. Shan *et al.* in Ref. 21 calculate the thermal time constant by considering a thermal resistor in analogy to RC circuits. They measure the quantity during the cooling period following a DC drive current. A similar experimental extraction of this time constant for AlGaIn/GaN HEMTs during pulsed operation is presented by Lancry *et al.* in Ref. 22.

During the low-current pulse of our junction temperature measurement, an immediate rise in forward voltage is observed, as shown in Fig. 5. This rise is attributed to cooling in the device as heat diffuses from the active region into the subsequent mounting layers and into the heat sink. This voltage data may be translated into a time-dependent temperature using the calibration data from Fig. 1(a). As discussed above, the time resolution in the electronics offers a means of observing the precise time dependence of the forward voltage within the first few milliseconds of the decay.

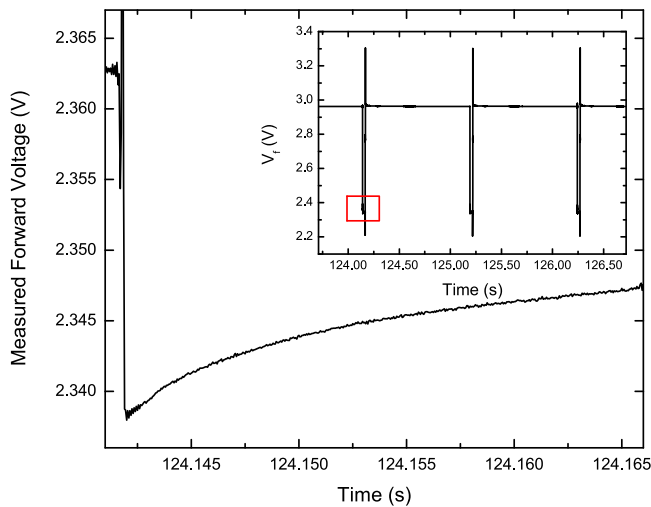


FIG. 5. (Color online) Output of DAQ voltmeter used to measure junction temperature. The inset demonstrates the region of the pulsed current plot used to extract the cooling in the device.

Previous investigators²¹ have used analogous results to estimate the thermal time constant, τ , by fitting temperature as a function of time with an exponential decay similar to Eq. (7). In agreement with these prior reports, the exponential

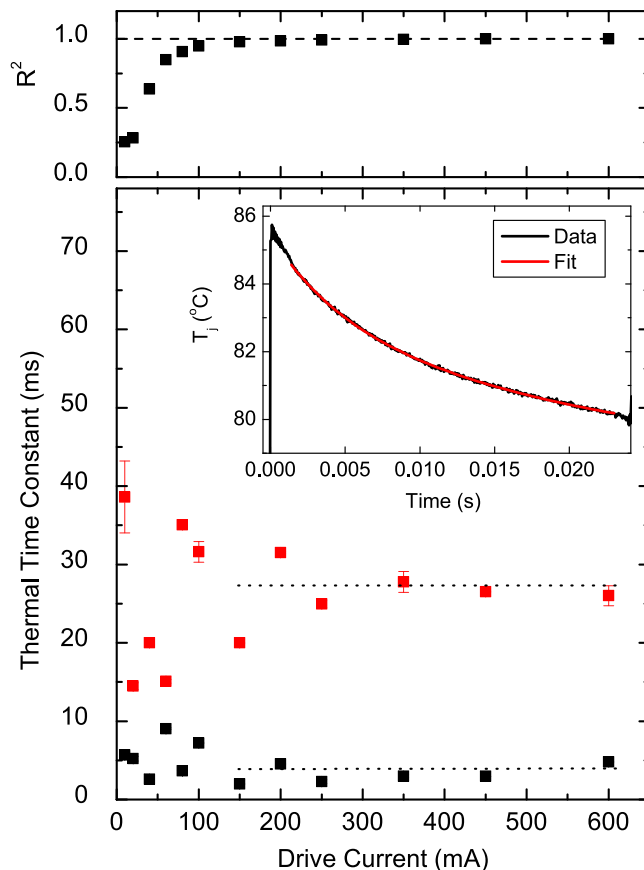


FIG. 6. (Color online) Plots of the measured thermal time constants for the LED. The dotted line indicates average values for the two time constants resulting from the fitting illustrated in the inset. The top panel shows R^2 values for each drive current.

decay model which best fits our data involves two time constants, of the form

$$T(t) = \beta_1 \exp\left(-\frac{(t-t_0)}{\tau_1}\right) + \beta_2 \exp\left(-\frac{(t-t_0)}{\tau_2}\right), \quad (8)$$

where τ_1 and τ_2 are the thermal time constants and t_0 is the time at which the drive-voltage is switched to begin the T_j measurement.

Figure 6 shows the thermal time constant results (lower panel) and R^2 of the fit for various drive conditions. It is apparent from the plot of R^2 that the fit is superior for higher drive currents, above 200 mA. This is expected, as the temperature difference from ambient is greatest at higher drive so the measured voltages are more significant. The dotted line is a guide to the eye for the two average thermal time constant values: $\tau_1 = 3.26 \pm 1.16$ ms and $\tau_2 = 26.1 \pm 3.77$ ms, which are in agreement with related studies for these materials,^{20,21} and the ratio $\beta_1/\beta_2 \sim 2$. The presence of two time constants can be attributed to the lateral and vertical heat flow through the LED chip itself, and then into underlying submount material, acting as parallel heat conduction paths from the device active region. This signifies that the experimental method presented here is a viable means of extracting the thermal time constant during operation and is prospectively useful for predicting failure during operation.

IX. CONCLUSIONS

In conclusion, the junction temperature for InGaN/GaN MQW high-brightness LEDs was determined using a straightforward forward voltage technique. The approach was checked up to a temperature rise of $\sim 90^\circ\text{C}$ above ambient in a commercial blue LED. The observed blue shift in the EL spectra, under typical drive conditions, confirms the presence of bandfilling and carrier screening in the polar III-N materials for these devices in addition to the ubiquitous self-heating. These combined effects preclude the use of EL for estimating temperature in these polar device materials. By comparing the behavior of the EL peak energy under high drive currents and at low-pulse currents, the extent of these competing effects was quantified. The presence of these effects on the peak output energy further confirms the efficacy of using an electrical technique such as the forward voltage method for accurate junction temperature measurements in III-N high-brightness LEDs. Finally, the forward voltage technique presented offers a means for experimentally extracting the thermal relaxation time for the device material. This method is applicable to nonpolar as well as polar LED and heterojunction devices.

¹S. Todoroki, M. Sawai, and K. Aiki, *J. Appl. Phys.* **58**, 1124 (1985).

²N. C. Chen, Y. N. Wang, C. Y. Tseng, and Y. K. Yang, *Appl. Phys. Lett.* **89**, 101114 (2006).

³Y. Xi *et al.*, *Appl. Phys. Lett.* **86**, 031907 (2005).

⁴Y. Xi and E. F. Schubert, *Appl. Phys. Lett.* **85**, 2163 (2004).

⁵A. Keppens, W. R. Ryckaert, G. Deconinck, and P. Hanselaer, *J. Appl. Phys.* **104**, 093104 (2008).

⁶Q. Chen, X. Luo, S. Zhou, and S. Liu, *Rev. Sci. Instrum.* **82**, 084904 (2011).

- ⁷J.-C. Wang, C.-H. Fang, Y.-F. Wu, W.-J. Chen, D.-C. Kuo, P.-L. Fan, J.-A. Jiang, and T.-E. Nee, *J. Lumin.* **132**, 429 (2012).
- ⁸J. Hulett and C. Kelly, *Photonics Spectra* **42**, 73 (2008).
- ⁹Y. P. Varshni, *Physica* **34**, 149 (1967).
- ¹⁰E. F. Schubert, *Light-Emitting Diodes* (Cambridge University, Cambridge, 2006).
- ¹¹R. Passler, *J. Appl. Phys.* **89**, 6235 (2001).
- ¹²M. E. Holtz, I. GherasoIU, V. Kuryatkov, S. A. Nikishin, A. A. Bernussi, and M. W. Holtz, *J. Appl. Phys.* **105**, 063702 (2009).
- ¹³D. Y. Song, M. Basavaraj, S. A. Nikishin, M. Holtz, V. Soukhoveev, A. Usikov, and V. Dmitriev, *J. Appl. Phys.* **100**, 113504 (2006).
- ¹⁴P. G. Eliseev, P. Perlin, L. Jinhyun, and M. Osinski, *Appl. Phys. Lett.* **71**, 569 (1997).
- ¹⁵K. L. Teo *et al.*, *Appl. Phys. Lett.* **73**, 1697 (1998).
- ¹⁶S. Nakagawa, H. Tsujimura, K. Okamoto, M. Kubota, and H. Ohta, *Appl. Phys. Lett.* **91**, 171110 (2007).
- ¹⁷C. Lu *et al.*, *J. Appl. Phys.* **113**, 013102 (2013).
- ¹⁸T. Mukai, D. Morita, and S. Nakamura, *J. Cryst. Growth* **189–190**, 778 (1998).
- ¹⁹T. Mukai, M. Yamada, and S. Nakamura, *Jpn. J. Appl. Phys., Part 2* **37**, L1358 (1998).
- ²⁰P. Vitta and A. Žukauskas, *Phys. Status Solidi C* **6**, S877 (2009).
- ²¹Q. Shan, Q. Dai, S. Chhajed, J. Cho, and E. F. Schubert, *J. Appl. Phys.* **108**, 084504 (2010).
- ²²O. Lancry, E. Pichonat, J. Réhault, M. Moreau, R. Aubry, and C. Gaquière, *Solid-State Electron.* **54**, 1434 (2010).